Int J Adv Manuf Technol (2018) 95:1293–1301
https://doi.org/10.1007/s00170-017-1273-2

ORIGINAL ARTICLE

# Thermal behavior analysis of horizontal CNC lathe spindle and compensation for radial thermal drift error

**Kuo Liu**[1] · **Te Li**[1] · **Tiejun Li**[2] · **Yu Liu**[2] · **Yongqing Wang**[1] · **Zhenyuan Jia**[1]

Received: 6 June 2017 / Accepted: 26 October 2017 / Published online: 9 November 2017


**Abstract** At present, the thermal deformation law of the horizontal CNC lathe spindle has not been observed, whereas no effective model for the radial thermal drift error for the CNC lathe spindle exists. In order to solve these problems, the thermal deformation of the spindle was investigated on a CNC lathe, and the temperatures along with the radial thermal drift errors of various rotation speeds were obtained. Based on the test result analysis, the radial thermal drift error mechanism and the complete thermal deformation during the warmup and cooldown phases were expounded. The "Liu-loop" of the spindle was drawn, and the corresponding two basic characteristics were described. Ten types of spindle thermal deformations are listed, and the relationship between the radial thermal drift error and the temperatures of the key points was established by a physically based modeling method. The criteria for the spindle thermal determination and the compensation value expression for the workpieces with various lengths were given. Finally, the effectiveness of the proposed model was proved by simulations and experiments.

**Keywords** Horizontal CNC lathe · Spindle · Thermal behavior · Thermal error · Compensation

✉ Te Li
teli@dlut.edu.cn

[1] Key Laboratory for Precision and Non-Traditional Machining Technology of Ministry of Education, Dalian University of Technology, Dalian 116024, China

[2] College of Mechanical Engineering and Automation, Northeastern University, Shenyang 110819, China

## 1 Introduction

The heat sources in a machine tool, such as the bearing rotation, the motor, the cooling system, and the ambient temperature, cause thermal deformation in the structure and lead to the machine thermal error [1]. The thermally induced error is a time-dependent nonlinear process. The interaction among the heat source location, the corresponding intensity, the thermal expansion coefficient, and the machine configuration creates complex thermal behaviors in the machine tools [2]. A high number of studies demonstrated that the thermal error accounts for 40–70% of the total errors of a machine tool; subsequently, it constitutes the key affecting factor on the machining accuracy [3].

Regarding the CNC lathe, it has two characteristics: (1) the spindle rotates continuously during machining; (2) the stroke of the servo axis is usually short. These two characteristics lead in the thermal error of the spindle accounting for a higher proportion of the total error, compared to the servo axis thermal error. The thermal error of the spindle consists of the axial thermal growth and the radial thermal drift error [4–6]. Many scholars have researched the modeling and compensation for the axial thermal growth of the spindle by directly mapping the thermal error against the temperature of the critical machine elements, consequently achieving good results [7–9]. Regarding the radial thermal drift error of the CNC lathe spindle, few studies can be found, due to the corresponding complex formation and thermal deformation. Babu et al. [10] addressed the issues of the thermal displacements in the headstock assembly of a slant bed CNC lathe. Both experimental and numerical investigations were executed, to gain insights into the extent of contribution made by the elements of the headstock assembly on the transient temperature increase and the resulting thermal deformation characteristics. Mori et al. [11] investigated an approach to reduce and compensate the

thermal displacement for high-accuracy NC lathes. Guo et al. [12] utilized the gray comprehensive correlation analysis method to identify the temperature-sensitive measurement points and constructed a thermal error prediction model based on the re-sampling step particle swam optimization to evaluate the compensation effect for the spindle system of a CNC lathe. Yang et al. [13] proposed three models of spindle thermal errors for the thermal yaw, pitch angles, and elongation and performed error compensation based on the thermal tilt angles and cutting tool length. Ma et al. [14] used genetic algorithm (GA) and particle swarm optimization (PSO) to optimize the parameters of ANNs with back propagation (BP) algorithm, and compensated the thermal yaw, pitch angles, and elongation of the spindle.

It could be observed from the present study that the thermal deformation law of the CNC lathe spindle was not presented, and the model of the radial thermal drift error was not established for the spindle of CNC horizontal lathe. In contrast, the radial error of the lathe spindle is quite important, because we are more concerned about the accuracy of the $X$ direction of the lathe. Therefore, this study was focused on the radial thermal drift error research of the horizontal CNC lathe spindle. Based on the thermal behavior test, the spindle entire thermal deformation of the horizontal CNC lathe was presented, and the radial thermal drift error model of the spindle was established and compensated.

## 2 Spindle thermal behavior investigation

### 2.1 Horizontal lathe and instrument

In order to investigate the thermal behavior of the spindle in a horizontal CNC lathe, the spindle thermal deformation was measured. The lathe acquired the structure of the flat bed and the 60° slant saddle. The mechanical spindle was mounted on the bed and driven through the belt, and the maximum rotation speed was 5000 rpm. The $X$-axis was mounted on the slant saddle.

The spindle thermal deformation was measured by a spindle error analyzer (Lion Precision Corporation, USA). The test bar had two precision balls, and the capacitive displacement sensors were fixed on the row-type tool holder through the fixture, aimed at the balls (Fig. 1). The distance between these two displacement sensors was determined by the fixture at 76.2 mm. The maximum testing speed of the spindle error analyzer was 60,000 rpm, and the sampling period for error was set at 10 s. According to the setting of the instrument, the error value appeared to be negative when the distance between the test bar and the displacement sensor became higher. Temperature sensors were utilized to measure the spindle key point temperatures. The temperature sensor chip was the Tsic506F of the IST Corporation in Switzerland; the sensors

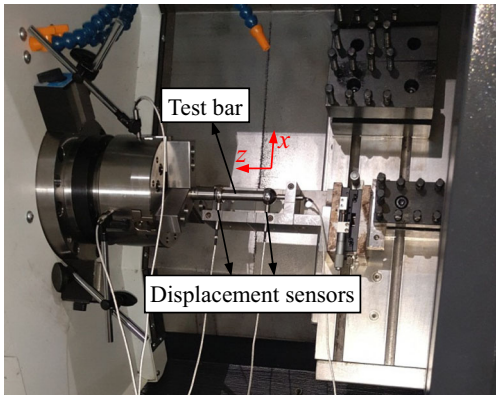


**Fig. 1** On-site test

were calibrated by Liaoning Institute of Measurement in China prior to utilization, and the expanded uncertainty was $U = 0.1$ °C (0–60 °C). The temperature sensor was produced from the magnetic material NdFeB, which could easily be attached to any ferrous material. A high number of sensors were arranged in various positions prior to the formal test, to find the sensitive points of the spindle thermal deformation. Finally, two temperature sensors, $T_1$ and $T_2$, were utilized in the positions presented in Fig. 2. The $T_1$ was utilized to represent the left side temperature of the headstock, whereas the $T_2$ was utilized to represent the right side temperature of the headstock. The sampling period for the temperature measurements was also set at 10 s.

### 2.2 Test results and analysis

The radial thermal drift errors and temperatures were assessed at the rotation speeds of 2000, 3000, and 4000 rpm, respectively. In each test, the spindle rotated at a preset rotation speed for 4 h to warm up and subsequently remained stopped for 3 h to cool down. The obtained results are presented in Fig. 3, where $e_{1,x}$ was the test result of the right displacement sensor and $e_{2,x}$ was the test result of the left displacement sensor.

It could be observed from Fig. 3 that the higher the rotation speed was, the higher the temperature increase of key points was and the higher the thermal drift errors were. In contrast, it could be observed from the error diagram that when the temperature increased, the error became to positive first, which was interpreted that the test bar moved downwards. But the spindle should not move down after rotation, so the thermal deformation of spindle may not be a simple upward translation. Similarly, the error became negative in an accelerated manner, when the spindle started to cool down, which was also interpreted that the spindle thermal deformation might not display a simple downward transition. The $T_1$ and $T_2$ temperatures were different, especially in the beginning of the warmup and cooldown phases, as it could be observed in Fig. 3. In addition, it could be observed through the error diagram that the difference between $e_{1,x}$ and $e_{2,x}$ was higher

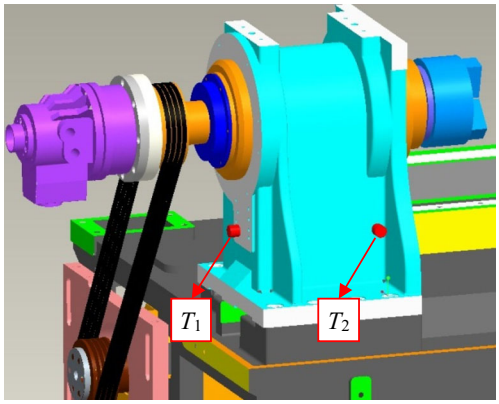


**Fig. 2** Temperature sensor locations

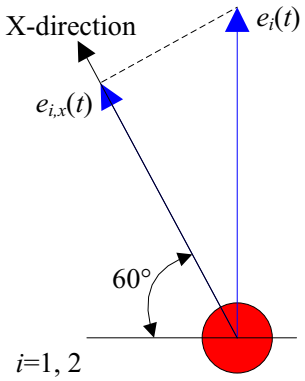


**Fig. 4** Radial thermal error component

in the beginning of the warmup and cooldown phases at the same speed. These phenomena indicated that the thermal tilt deformation occurred in the spindle.

### 2.3 "Liu-loop" and thermal deformation of spindle

Since the lathe adopted the structure of the 60° slant saddle, the thermal expansion of the spindle along the vertical direction $e_i$ ($i$ = 1, 2) had a $X$-directional thermal error component $e_{i,x}$, as presented in Fig. 4. Therefore, the $X$-directional thermal error components $e_{1,x}$ and $e_{2,x}$ are:

$$e_{2,x} = \sin(\pi/3) \times e_2 \quad (1)$$

$$e_{1,x} = \sin(\pi/3) \times e_1 \quad (2)$$

The relationship between the temperature difference ($T_1 - T_2$) and the thermal tilt angle $\varphi_s$ is presented in Fig. 5. The thermal tilt angle $\varphi_s$ is calculated by Eq. (3):

$$\phi_s = \arctan\frac{e_{1,x} - e_{2,x}}{\sin(\pi/3) \times 1000 \times 76.2} \quad (3)$$

It can be surmised from Fig. 5 that the correlation between the temperature difference ($T_1 - T_2$) and the thermal tilt angle $\varphi_s$ was significantly strong, further demonstrating that the spindle indeed thermally tilted by the temperature difference between the left and right sides of the spindle. Furthermore, the relationships between the error $e_{1,x}$ and the temperature difference at various speeds are presented in Fig. 6.

As can be observed from Fig. 6, the relationship between the radial thermal drift error and the temperature difference formed an approximate ring, which was called a "Liu-loop." All types of machine tool spindles, including the mechanical spindle and the electric spindle, display a "Liu-loop" during warmup and cooldown. The "Liu-loop" has two basic characteristics:

(1) When the spindle cooldown duration is sufficiently high, the "Liu-loop" will be closed.
(2) The higher the spindle rotation speed is, the higher the "Liu-loop" is.

The thermal deformation of the CNC lathe spindle was expounded with the combination of the "Liu-loop," further:

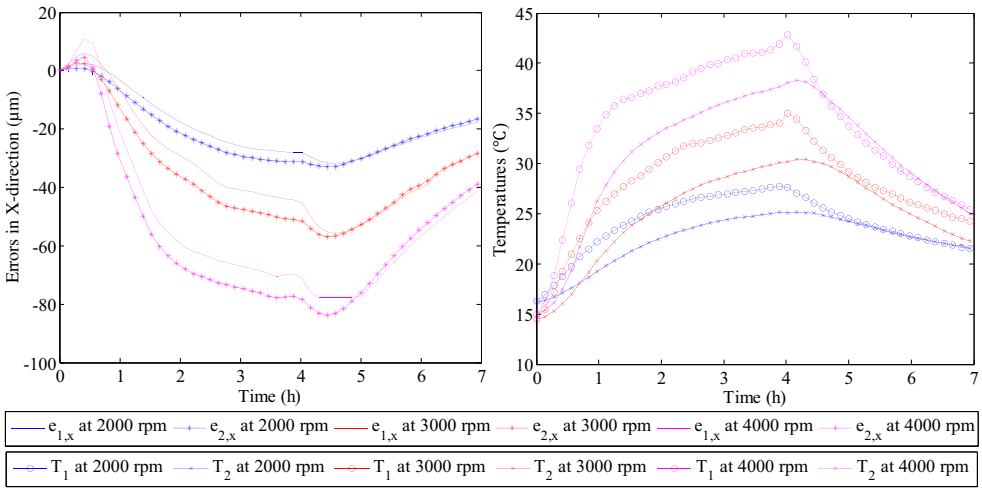


**Fig. 3** Errors and temperatures of various rotation speeds

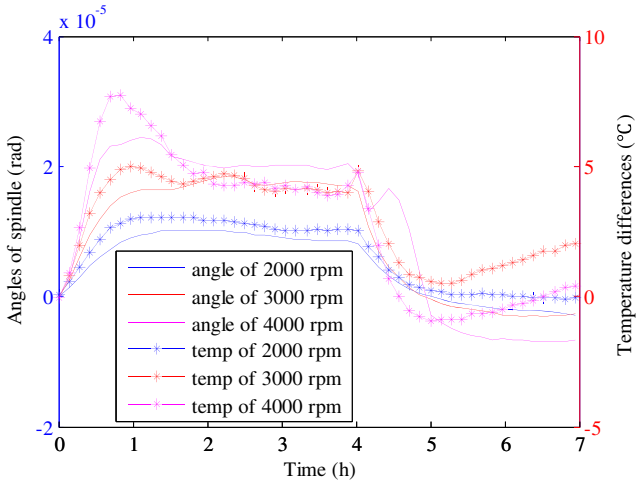


**Fig. 5** Temperature difference and thermal angle relationship

(1) The spindle started to rotate, and the left side of the headstock warmed up rapidly, due to the heat from the rear bearing and the belt. In contrast, the temperature of the headstock right side had not yet increased. The temperature difference between the left and right sides rapidly increased; the spindle tilted and the tilt angle became rapidly higher. The test bar tilted downwards and almost reached the displacement sensors; therefore, both $e_{1,x}$ and $e_{2,x}$ gradually acquired a positive value, with $e_{1,x} > e_{2,x}$.

(2) Subsequently to a period of rotation, the temperature gradients of the headstock both sides were gradually stable; therefore, the temperature difference in Fig. 6 was quite low. In contrast, the temperatures of both sides were still increasing (Fig. 3). As a result, the headstock expanded upwards along with the spindle; the test bar moves further away from the displacement sensors, and both $e_{1,x}$ and $e_{2,x}$ gradually acquired negative values.

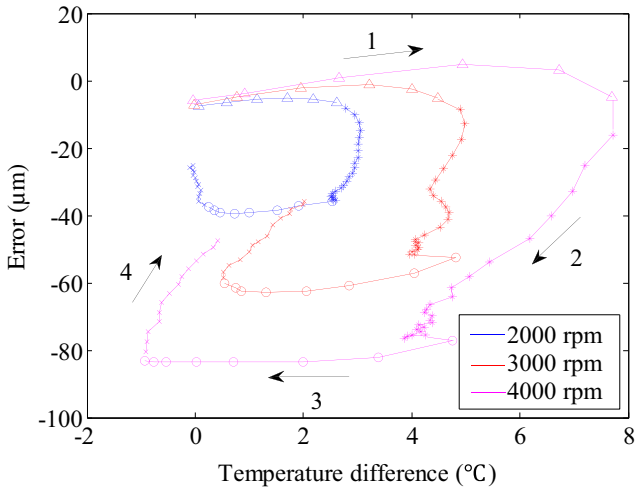


**Fig. 6** "Liu-loop" of spindle

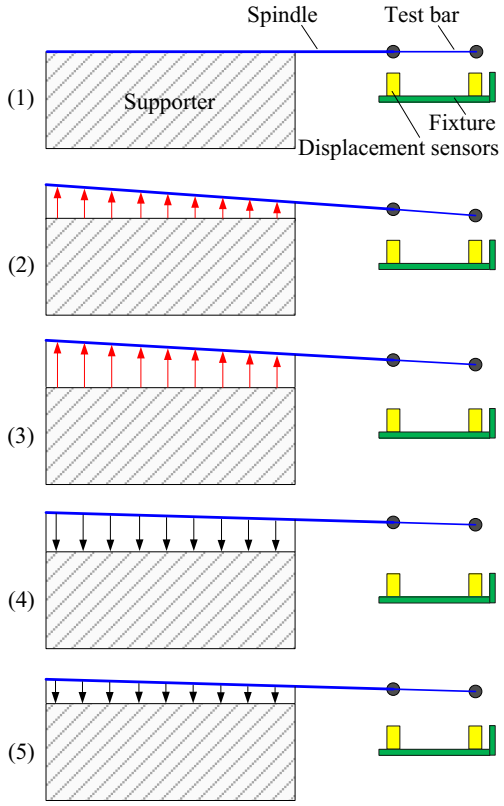


**Fig. 7** Spindle thermal deformation

(3) The spindle stopped the rotation. The headstock began to cool down, and the temperature of the left side decreased more rapidly than the right side temperature. Therefore, the temperature difference between both sides was rapidly reduced. The tilt angle of the spindle also decreased rapidly; therefore, the test bar still moved further away from the displacement sensors.

(4) After rotation had stopped for a period of time, the temperature gradient of the headstock became gradually stable; subsequently, the temperature difference in Fig. 6 was quite low. In contrast, the temperatures of both sides were still decreasing (Fig. 3). As a result, the headstock thermally shrunk downwards along with the spindle, and the test bar moved closer to the displacement sensors. Due to insufficient cooling duration, the spindle did not return to the thermal equilibrium state; subsequently, both $e_{1,x}$ and $e_{2,x}$ did not return to 0 at the last testing time frame, and the "Liu-loop" did not close.

The entire thermal deformation of the spindle and the headstock during warmup and cooldown is presented in Fig. 7: The (1) represents the initial thermal stability. The (2) represents the state following warmup for a short duration. The (3) represents the state following warmup for a longer period of time. The (4) represents the state following cooldown for a short

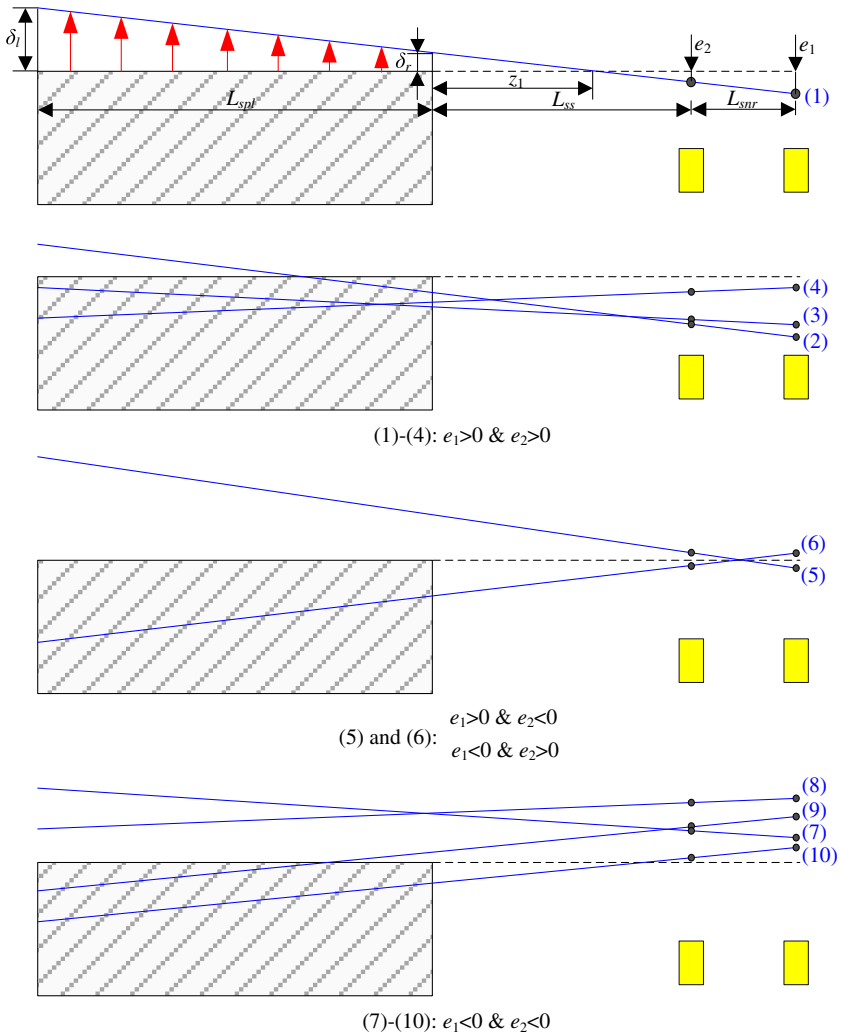


**Fig. 8** Thermal postures of spindle

period of time. The (5) represents the state following cool-down for a longer period of time.

**Table 1** Determination criteria for thermal postures

| Postures | $\delta_l$ and $\delta_r$ | $L_\sigma$ |
|---|---|---|
| 1 | $\delta_l > \delta_r \geq 0$ | $L_\sigma \leq L_{ss}$ |
| 2 | $\delta_r < 0 < \delta_l$ | |
| 3 | $\delta_r \leq \delta_l < 0$ | |
| 4 | $\delta_l < \delta_r < 0$ | $L_{ss} + L_{snr} < L_\sigma$ |
| 5 | $\delta_l > \delta_r \geq 0$ | $L_{ss} < L_\sigma \leq L_{ss} + L_{snr}$ |
| 6 | $\delta_l < \delta_r < 0$ | $L_{ss} < L_\sigma \leq L_{ss} + L_{snr}$ |
| 7 | $\delta_l > \delta_r \geq 0$ | $L_{ss} + L_{snr} < L_\sigma$ |
| 8 | $\delta_r \geq \delta_l \geq 0$ | |
| 9 | $\delta_l < 0 < \delta_r$ | |
| 10 | $\delta_l < \delta_r < 0$ | $L_\sigma \leq L_{ss}$ |

## 3 Thermal deformation model of spindle

In Section 2.3, the mechanism and cause of the thermal behavior of the horizontal CNC lathe spindle were analyzed, and the entire thermal deformation of the spindle was expounded. In this section, the modeling for radial thermal drift error was studied based on the analysis in Section 2.3. The physically based modeling method in the thermal error compensation became a major research direction in accuracy control. This occurred because the data-driven modeling method required sufficient data to represent the input-output relationships associated with the process, and the corresponding major disadvantage was the poor robustness. In contrast, the physically based modeling method advantage was that the model was designed based on the constitutive model; therefore, the model robustness was strong, and the prediction accuracy of the model was high. According to the aforementioned analysis, the relationship between the radial thermal drift error and the temperatures of the key points was established by the physically based modeling method.

**Table 2** Identified parameters

| Parameters | Values |
|---|---|
| $\alpha_l$ | 5.256 |
| $\beta_l$ | 2 |
| $\alpha_r$ | 4.368 |
| $\beta_r$ | 2 |

The horizontal CNC lathe spindle and the instrument at the thermal equilibrium state are presented in Fig. 7 (1). Although Fig. 7 presents the spindle thermal deformation during warmup and cooldown, however, during the practical machining process, the thermal deformation might not follow these postures. As an example, if the ambient temperature decreases, or the setting temperature of the cooling system is lower than the ambient temperature, it might cause the headstock to shrink. Therefore, it was necessary to analyze all possible thermal deformation postures. The thermal deformation postures of the spindle could be divided into three categories and ten low-sized actions, as presented in Fig. 8.

In Fig. 8, the $\delta_l$ was the thermal error of the headstock left side, and the $\delta_r$ was the thermal error of the headstock right side. Both $\delta_l$ and $\delta_r$ were positive at thermal expansion and negative at thermal shrinkage. The $z_1$ was the distance between the right side of the headstock and the crossover point, which was crossed by the deformed spindle and the original spindle. The $L_{spl}$ was the horizontal distance between the left and right sides of the headstock. The $L_{ss}$ was the horizontal distance between the headstock right side and the left displacement sensor. The $L_{snr}$ was the horizontal distance between these two displacement sensors.

With the thermal deformation (1) of Fig. 8 consideration as an example, the relationship between the radial thermal drift error and the temperature was established. Although the temperatures of the left and right sides of the headstock were different, the temperature field was continuous and approximately linear. Therefore, the linear relationship between the thermal expansion and the temperature was established for both sides of the headstock, and the temperature was utilized

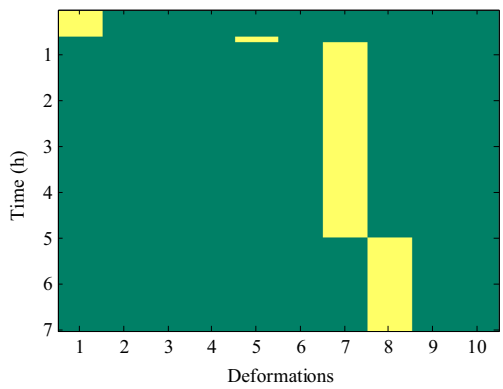


**Fig. 9** Deformation change graph at 4000 rpm

to represent the dynamic change of the headstock thermal expansion. The model could be expressed by Eqs. (4) and (5):

$$\delta_l(t) = \alpha_l \times (T_1(t) - T_1(0)) + \beta_l \tag{4}$$

$$\delta_r(t) = \alpha_r \times (T_2(t) - T_2(0)) + \beta_r \tag{5}$$

where, $\alpha_l$, $\alpha_r$, $\beta_l$, and $\beta_r$ are the coefficients to be identified.

Equation (6) could be obtained from the triangular proportional relationship:

$$\frac{z_1}{\delta_r} = \frac{L_{spl}}{\delta_l - \delta_r} \tag{6}$$

Through the Eq. (6) conversion and the $z_1(t)$ at time $t$, it could be expressed as:

$$z_1(t) = \frac{L_{spl} \times \delta_r(t)}{\delta_l(t) - \delta_r(t)} \tag{7}$$

Furthermore, the thermal expansion of the spindle along the vertical directions $e_1(t)$ and $e_2(t)$ at time $t$ could be expressed as:

$$e_2(t) = \frac{(\delta_l(t) - \delta_r(t))(L_{spl} + L_{ss}) - L_{spl}\delta_l(t)}{L_{spl}} \tag{8}$$

$$e_1(t) = \frac{(\delta_l(t) - \delta_r(t))(L_{spl} + L_{ss} + L_{snr}) - L_{spl}\delta_l(t)}{L_{spl}} \tag{9}$$

The $e_{1,x}$ and $e_{2,x}$ can be obtained by Eqs. (1) and (2). The derivation of the models for Fig. 8 (2)–(10) were referred to Fig. 8 (1).

The spindle might start and stop irregularly during machining, possibly changing dynamically among these ten types of thermal deformation. Since the displacement sensors could not be utilized to monitor the thermal deformation of the spindle during machining, all $\delta_l$, $\delta_r$, and $L_\sigma$ were utilized in the real-time thermal deformation determination. The $L_\sigma$ was the distance between the headstock right side and the crossover point, which was crossed by the deformed spindle and the original spindle. For all types of thermal deformation, the $L_\sigma$ calculation could be expressed as follows:

$$L_\sigma = L_{spl} \times \left| \frac{\alpha_r \Delta T_2(t) + \beta_r}{\alpha_l \Delta T_1(t) - \alpha_r \Delta T_2(t) + \beta_l - \beta_r} \right| \tag{10}$$

Table 1 presents the determination criteria for the thermal postures during machining.

Because the thermal tilt deformation exists in the spindle system, the thermal deformation value varies according to the workpiece length. The $L_{wp}$ was set as the distance between the

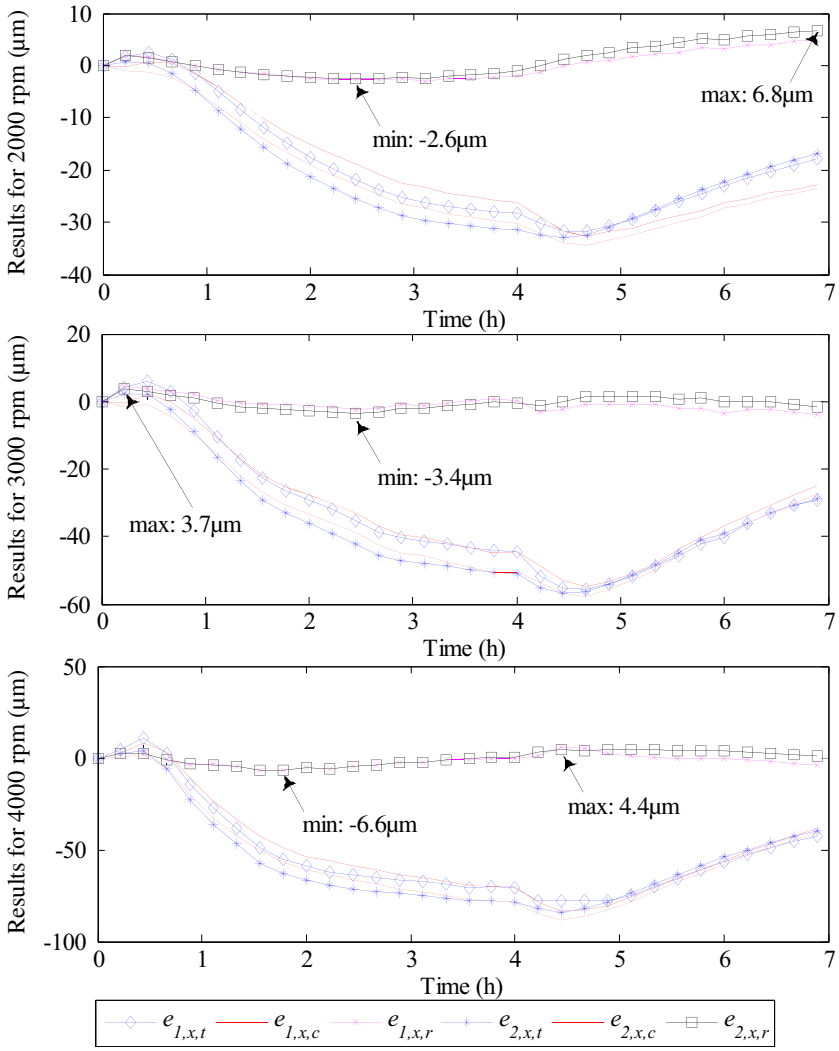


**Fig. 10** Simulation results for various rotating speeds

end of the spindle and the cutting position on the workpiece. The $L_s$ was set as the distance between the end of the spindle and the left displacement sensor. For all types of thermal deformation, presented in Fig. 8, such as for $L_{wp} > L_s + 76.2$, $L_s < L_{wp} < L_s + 76.2$, and $L_{wp} < L_s$, the compensation value for the cutting position on the workpiece could be expressed as follows:

$$e_{wp} = e_{2,x} - \frac{(e_{1,x} - e_{2,x})(L_s - L_{wp})}{1000 \times 76.2} \tag{11}$$

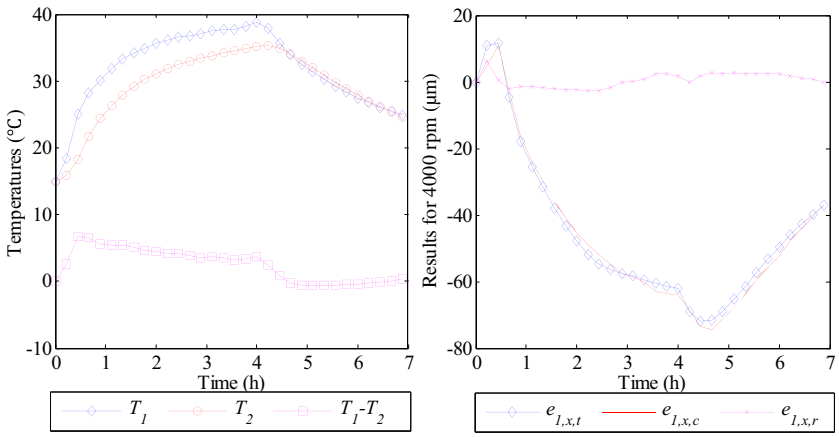


**Fig. 11** Temperatures and prediction results for 4000 rpm

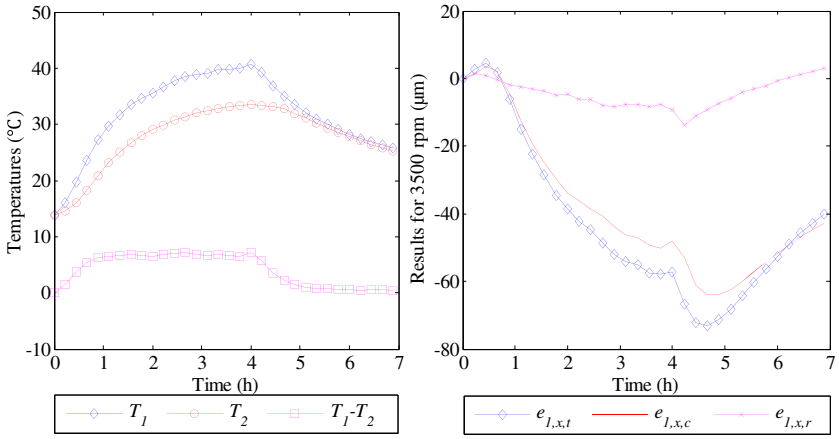


**Fig. 12** Temperatures and prediction results for 3500 rpm

## 4 Validation

### 4.1 Parameter identification and simulations

The parameters, $\alpha_l$, $\alpha_r$, $\beta_l$, and $\beta_r$, were required to be identified. The $\delta_l$ and the $\delta_r$ could be obtained by a backward deduction through the tested values of $e_{1,x,t}$ and $e_{2,x,t}$. Therefore, regarding Eqs. (4) and (5), the corresponding independent variables $T_1$ and $T_2$ and the dependent variables $\delta_l$ and $\delta_r$ were all acquired. The parameters were identified by the least square method, and the results are presented in Table 2.

The prediction effect of the proposed model was simulated in Matlab with the parameters in Table 1. Figure 9 presents the thermal deformation posture change graph of the spindle at 4000 rpm, and this was obtained based on the determination criteria for the thermal postures. It could be observed that the spindle changed among postures (1), (5), (7), and (8) during the warmup for 4 h and the cooldown for 3 h at 4000 rpm. This was different from the thermal deformation analyzed in section 2, whereas the difference was slight.

Figure 10 presents the simulation results for various rotation speeds, where, $e_{1,x,t}$ is the tested value of $e_{1,x}$, $e_{1,x,c}$ is the calculated value of $e_{1,x}$, $e_{1,x,r}$ is the simulation residual error of $e_{1,x}$, $e_{2,x,t}$ is the tested value of $e_{2,x}$, $e_{2,x,c}$ is the calculated value of $e_{2,x}$, and $e_{2,x,r}$ is the simulation residual error of $e_{2,x}$. It could be observed from the results that the error with compensation was significantly lower than that the error without compensation.

### 4.2 Experiments

The horizontal CNC lathe was tested once again at 4000 and 3500 rpm, respectively. Also, the temperature and the thermal error of the spindle were measured by a temperature sensor and a spindle error analyzer, respectively. The prediction results of the model are presented in Figs. 11 and 12.

It could be observed from Figs. 11 and 12 that when the spindle rotation speed was similar to the modeling test speed, the model prediction effect was quite good. Even when the spindle rotation speed differed from the modeling test speed, the prediction effect of the model was good whereas not as good at the same rotation speed. This occurred due to the slight difference in the thermal behaviors of the spindle at various speeds.

## 5 Conclusions

Both the thermal deformation mechanism and the process of the horizontal CNC lathe spindle were presented, and the prediction model for the radial thermal drift error was established. The simulation effect was validated by both simulations and experiments, where the compensation problem for the radial thermal drift error was solved. The advantages of this compensation method were as follows: (1) only two temperature sensors were utilized; (2) the test efficiency was high, and only one test at a certain speed was required for the model; and (3) the model was robust to various rotation speeds. Moreover, the displayed thermal deformation mechanism and the process could provide an important reference for the spindle thermal-structure optimization design.

**Acknowledgements** This project are supported by National Natural Science Foundation of China (Grant No. 51775085), National Natural Science Foundation of China (Grant No. U1608251) and the Fundamental Research Funds for the Central Universities (DUT16RC(3)122). Moreover, the authors thank the anonymous referees and editor for their valuable comments and suggestions.

## References

1. Zhang T, Ye WH, Liang RJ, Lou PH, Yang XL (2013) Temperature variable optimization for precision machine tool thermal error compensation on optimal threshold. Chin J Mech Eng 26(1):158–165

2. Jin C, Wu B, YM H (2015) Temperature distribution and thermal error prediction of a CNC feed system under varying operating conditions. Int J Adv Manuf Technol 77(9–12):1979–1992
3. Ferreira PM, Liu CR (1993) Method for estimating and compensating quasistatic errors of machine tools. J Eng Ind 115(1):149–159
4. Liu K, Sun MJ, Zhu TJ, YL W, Liu Y (2016) Modeling and compensation for spindle's radial thermal drift error on a vertical machining center. Int J Mach Tools Manuf 105:58–67
5. Huang P, Lee WB, Chan CY (2016) Investigation on the position drift of the axis average line of the aerostatic bearing spindle in ultra-precision diamond turning. Int J Mach Tools Manuf 108:44–51
6. Guo C, Sun QH (2005) Analysis of thermal characteristics and thermal deformation of high-speed spindle system in NC precision lathe. J Southeast Univ 35(2):231–234
7. Tseng PC, Ho JL (2002) A study of high-precision CNC lathe thermal errors and compensation. Int J Adv Manuf Technol 19(11):850–858
8. Wu H, Zhang HT, Guo QJ, Wang XS, Yang JG (2008) Thermal error optimization modeling and real-time compensation on a CNC turning center. J Mater Process Technol 207(1–3):172–179
9. Liu K, Liu Y, Sun MJ, Li XL, Wu YL (2016) Spindle axial thermal growth modeling and compensation on CNC turning machines. Int J Adv Manuf Technol 87(5–8):2285–2292
10. Babu SR, Raja VP, Thyla PR, Thirumalaimuthukumaran M (2014) Prediction of transient thermo-mechanical behavior of the headstock assembly of a CNC lathe. Int J Adv Manuf Technol 74(1–4):17–24
11. Mori M, Mizuguchi H, Fujishima M, Ido Y, Mingkai N, Konishi K (2009) Design optimization and development of CNC lathe headstock to minimize thermal deformation. CIRP Ann Manuf Technol 58(1):331–334
12. Guo CG, Han X, Li Y, Xie HL (2016) Thermal error modeling for spindle system of precision CNC lathe. Opt Precis Eng 24(7):1731–1742
13. Yang J, Mei X, Zhao L, Feng B (2015) Thermal error compensation on a computer numerical control machine tool considering thermal tilt angles and cutting tool length. Proc Inst Mech Eng B J Eng Manuf 229:78–97
14. Ma C, Zhao L, Mei X, Shi H, Yang J (2017) Thermal error compensation of high-speed spindle system based on a modified BP neural network. Int J Adv Manuf Technol 89(9–12):3071–3085